

Preference-Conditioned Gradient Variations for Multi-Objective Quality-Diversity

HANNAH JANMOHAMED, Imperial College London, InstaDeep, UK

MAXENCE FALDOR, Imperial College London, UK

THOMAS PIERROT, InstaDeep, USA

ANTOINE CULLY, Imperial College London, UK

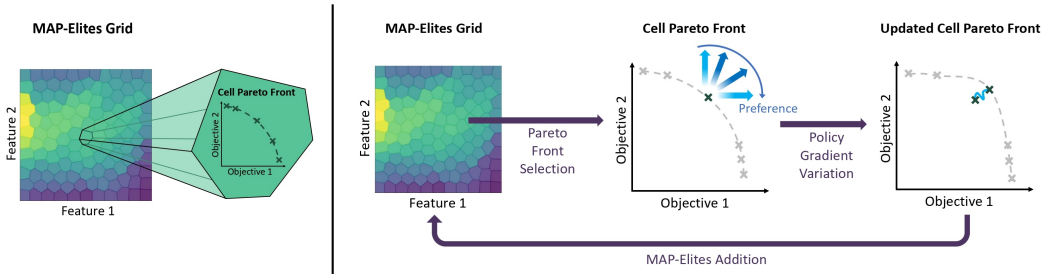


Fig. 1. *Left.* Multi-Objective MAP-Elites repertoire. The feature space $C \subset \mathbb{R}^d$ is tessellated into cells C_i . A set of non-dominated solutions is stored in each cell. The aim of moQD algorithms is to fill each cell with solutions that are Pareto-optimal. *Right.* Overview of preference-conditioned policy gradient in the MOME-P2c algorithm. By conditioning policy-gradients on updates solutions can be improved toward achieving different trade-offs of objectives (illustrated by blue arrows). By contrast, in MOME-PGx, solutions are only updated to improve performance on each objective separately (illustrated by light blue arrows).

In a variety of domains, from robotics to finance, Quality-Diversity algorithms have been used to generate collections of both diverse and high-performing solutions. Multi-Objective Quality-Diversity algorithms have emerged as a promising approach for applying these methods to complex, multi-objective problems. However, existing methods are limited by their search capabilities. For example, Multi-Objective Map-Elites depends on random genetic variations which struggle in high-dimensional search spaces. Despite efforts to enhance search efficiency with gradient-based mutation operators, existing approaches consider updating solutions to improve on each objective separately rather than achieving desired trade-offs. In this work, we address this limitation by introducing Multi-Objective Map-Elites with Preference-Conditioned Policy-Gradient and Crowding Mechanisms: a new Multi-Objective Quality-Diversity algorithm that uses preference-conditioned policy-gradient mutations to efficiently discover promising regions of the objective space and crowding mechanisms to promote a uniform distribution of solutions on the non-dominated front. We evaluate our approach on six robotics locomotion tasks and show that our method outperforms or matches all state-of-the-art Multi-Objective Quality-Diversity methods in all six, including two newly proposed tri-objective tasks. Importantly, our method also achieves a smoother set of trade-offs, as measured by newly-proposed sparsity-based metrics.

CCS Concepts: • **Theory of computation** → **Evolutionary algorithms**; • **Applied computing** → **Multi-criterion optimization and decision-making**; • **Computer systems organization** → **Evolutionary robotics**.

Authors' Contact Information: [Hannah Janmohamed](#), Imperial College London, InstaDeep, London, UK; [Maxence Faldor](#), Imperial College London, London, UK; [Thomas Pierrot](#), InstaDeep, Boston, USA; [Antoine Cully](#), Imperial College London, London, UK.

© 2026 Copyright held by the owner/author(s). Publication rights licensed to ACM.

This is the author's version of the work. It is posted here for your personal use. Not for redistribution. The definitive Version of Record was published in , <https://doi.org/10.1145/nnnnnnnn.nnnnnnnn>.

Additional Key Words and Phrases: Quality-Diversity, Multi-Objective Optimisation, MAP-Elites, Neuroevolution

ACM Reference Format:

Hannah Janmohamed, Maxence Faldor, Thomas Pierrot, and Antoine Cully. 2026. Preference-Conditioned Gradient Variations for Multi-Objective Quality-Diversity. 1, 1 (February 2026), 28 pages. <https://doi.org/10.1145/nnnnnnn.nnnnnnn>

1 Introduction

Over recent years, Deep Reinforcement Learning (RL) has enabled breakthroughs in mastering games [Mnih et al. 2013; Silver et al. 2016] as well as continuous control domains for locomotion [Cheng et al. 2024; Smith et al. 2022] and manipulation [OpenAI et al. 2019]. These milestones have demonstrated the extraordinary potential of RL algorithms to solve specific problems. However, most approaches return only one highly-specialised solution to a single problem. In contrast, there is a growing shift in focus towards not just uncovering one single solution that achieves high rewards, but instead many solutions that exhibit different ways of doing so [Zahavy et al. 2023]. Within this context, Quality-Diversity (QD) algorithms [Cully and Demiris 2018] have emerged as one promising approach for tackling this challenge.

In QD, the primary goal is to produce a variety of high-quality solutions, rather than to focus exclusively on finding the single best one. One motivation for QD algorithms is that, finding many solutions can provide availability of alternative, back-up solutions in the event that the highest-performing solution is no longer suitable. For example, in robotics, generating large collections of solutions has been shown to be helpful for addressing large simulation to reality gaps [Cully et al. 2015] and adapting to unforeseen damages [Allard et al. 2023; Cully et al. 2015]. Alternatively, having multiple solutions can simply be used in order to promote innovation in the downstream task. In this context, QD has been used for creating diverse video game levels [Bhatt et al. 2022; Khalifa et al. 2018] and generating building designs [Gaier et al. 2022].

Despite the growing traction of QD, most research in this field has focused on single-objective applications. However, multi-objective (MO) problems pervade many real-world domains, including engineering [Ferreira et al. 2019; Verstraeten et al. 2021], finance [Krasheninnikova et al. 2019], and drug design [Horwood and Noutahi 2020] and many state-of-the-art MO algorithms originate from the Evolutionary Algorithm community [Deb et al. 2000; Zhang and Li 2007; Zitzler et al. 2001; Zitzler and Thiele 1998].

Recently, Multi-Objective MAP-Elites algorithm (MOME) [Pierrot et al. 2022b] marked the first attempt at bridging ideas from QD and MO optimisation. In MOQD, the overarching goal is to identify a broad collection of solutions that exhibit diverse features *and* achieve distinct performances across multiple objectives. More specifically, given a feature space that is tessellated into cells, the aim is to find a collection of solutions within each cell which offer different trade-offs on each of the objectives (see Figure 1). As an example, consider the task of designing building sites. Within this context, it may be interesting to find different designs that vary in the number of buildings on the site. Then for each possible number of buildings, further options can be generated which present different trade-offs of ventilation and noise levels [Gaier et al. 2022]. This approach equips end-users with a spectrum of viable options, thereby broadening their perspective on the array of feasible design possibilities.

The MOME algorithm demonstrated promising results in finding large collections of diverse solutions that balance multiple objectives. However, MOME predominantly depends on random genetic variations that can cause slow convergence in large search spaces [Flageat et al. 2022; Nilsson and Cully 2021; Pierrot et al. 2022a]. This renders it less suitable for evolving neural networks with a large number of parameters.

Since the inception of the MOME framework, several related works exploring the domain of MOQD have emerged [Dean and Cheney 2023; Gaier et al. 2022; Janmohamed et al. 2023]. Among them, MOME-PGX [Janmohamed et al. 2023] builds upon the MOME framework and was shown to achieve state-of-the-art performance on high-dimensional continuous control robotics tasks that can be framed as Markov Decision Processes. It uses crowding addition and selection mechanisms to encourage an even distribution of solutions on the non-dominated front and employs policy-gradient mutations for each objective function in order to drive the exploration process toward promising regions of the solution space. However, the MOME-PGX approach is not without its own set of challenges. Firstly, it employs separate actor-critic networks for each objective function, which can be resource-intensive and may not scale with an increasing number of objectives. Furthermore, although using policy gradient-based updates helps with exploration in high-dimensional search spaces, the approach in MOME-PGX only considers improving solutions on each objective separately. However, in the context of multi-objective problems, the goal is often not just to maximise each objective independently but rather to find solutions which offer different trade-offs among them. In this way, if end users have different *preferences* regarding the relative importance of each objective, they have a range of solutions to choose from.

In this paper, we address the limitations of MOME-PGX by introducing a new MOQD algorithm: **Multi-Objective Map-Elites with Preference-Conditioned Policy-Gradient and Crowding Mechanisms** (MOME-P2C). Rather than using a separate actor-critic framework for each objective, MOME-P2C uses a single preference-conditioned actor and a single preference-conditioned critic. Similar to MOME-PGX, the actor-critic framework in MOME-P2C can be used to provide policy-gradient mutations which offer efficient search space exploration for high-dimensional neural-network policies. However, as illustrated in Figure 1, by conditioning the actor and critic networks on a preference, policy-gradient updates can be used to improve solutions toward achieving a given weighting over the objectives, rather than improve solutions on each objective disjointly. Moreover, using a single preference-conditioned actor-critic framework rather than one per objective also reduces training costs associated with maintaining the separate actor-critic networks of MOME-PGX.

We show that MOME-P2C outperforms or matches the performance of MOME-PGX across six robotic control MOQD tasks, including newly introduced tri-objective ones (see Section 5.1). MOME-P2C also outperforms MOME-PGX on two newly introduced sparsity-based MOQD metrics (see Section 5.3) demonstrating that it is able to attain a smoother set of trade-offs than MOME-PGX. The code for MOME-P2C is fully containerised and available at <https://github.com/adaptive-intelligent-robotics/MOME-P2C.git>.

2 Background

2.1 Quality-Diversity

Quality-Diversity algorithms aim to discover collections of solutions that are both high-performing and diverse [Pugh et al. 2016]. Similar to standard optimisation algorithms, a solution $\theta \in \Theta$ is assessed via a fitness function $f : \Theta \rightarrow \mathbb{R}$ that reflects its performance on the task. For example, consider the task of generating an image of a celebrity from a text prompt. In this case, the fitness of a solution could be the CLIP score [Radford et al. 2021] which measures the fidelity of an image to its caption that was used to generate it. However, an additional central component to QD algorithms, is the concept of the feature function $\Phi : \Theta \rightarrow \mathbb{R}^d$ that characterizes solutions in a meaningful way for the type of diversity desired [Pugh et al. 2016]. The feature of a solution $\Phi(\theta_i)$ is a vector that captures some of its notable characteristics, which is then consequently used to quantify its novelty relative to other solutions. In the image generation example, the feature could be the hair length or age of the subject in the photo [Fontaine and Nikolaidis 2023]. In this example, the QD algorithm

would then aim to generate images in which the subject has a diverse range of hair lengths and ages, and which closely obey the given text prompt used to generate it.

One branch of algorithms in the QD family stems from the MAP-ELITES algorithm [Mouret and Clune 2015], which has gained prominence for its simplicity and effectiveness. MAP-ELITES operates by discretising the feature space into a grid-like structure, where each cell C_i of the grid becomes a “niche” that can be occupied by a solution. Tessellating the feature space in this manner creates a systematic method for exploring of different niches within this space [Vassiliades et al. 2018]. Each iteration of MAP-ELITES first involves selecting solutions from these niches, creating copies of them and mutating these copies to create new candidate solutions. Then, the fitness and features of the candidate solutions are evaluated, and they are added to the appropriate niches based on their fitness. If the cell corresponding to the new solution’s feature vector is unoccupied, the new solution is added to the cell. If the cell is occupied, but the evaluated solution has a higher fitness than the current occupant, it is added to the grid. Otherwise, the solution is discarded. This process continues for a fixed number of iterations, progressively populating the grid structure with an array of diverse, high-quality solutions.

MAP-ELITES algorithms aim to maximise the total number of occupied cells at the end of the process and the performance of the solutions within each of them. Given a search space Θ and a feature space C that has been tessellated into k cells C_i , the MAP-ELITES objective, or QD-score [Cully and Demiris 2018] can be formally expressed as:

$$\max_{\theta \in \Theta} \sum_{i=1}^k f(\theta_i), \text{ where } \forall i, \Phi(\theta_i) \in C_i. \quad (1)$$

2.2 Multi-Objective Optimisation

Multi-Objective (MO) optimisation provides an approach for addressing problems that involve the simultaneous consideration of multiple, often conflicting objectives $\mathbf{F} = [f_1, \dots, f_m]$. In MO problems, objectives often compete with each other, meaning that improving one objective typically comes at the expense of another. For example, in engineering, improving performance might increase cost, and vice versa. To navigate this landscape, the concept of Pareto-dominance is commonly employed to establish a preference ordering among solutions. A solution θ_1 is said to dominate another solution θ_2 if it is equal or superior in at least one objective and not worse in any other [Hayes et al. 2022]. That is, $\theta_1 \succ \theta_2$, if $\forall i : f_i(\theta_1) \geq f_i(\theta_2) \wedge \exists j : f_j(\theta_1) > f_j(\theta_2)$.

Solutions that are not dominated by any other solutions are termed *non-dominated*. Given a set of candidate solutions \mathcal{S} , the non-dominated solutions of this set $\theta_i \in \mathcal{S}$ collectively form a *non-dominated front*, which represents the boundary of achievable trade-offs among objectives. The goal of MO optimisation is to find an approximation to the *optimal Pareto front*, i.e., the non-dominated front over the entire search space Θ .

There are two metrics, the hypervolume and sparsity metric (see Figure 2), that play pivotal roles in comprehensively assessing the quality and diversity of solutions within a Pareto front approximation [Cao et al. 2015; Hayes et al. 2022]. The hypervolume Ξ of a front \mathcal{P} , measures the volume of the objective space enclosed by a set of solutions relative to a fixed reference point r . This metric provides a quantitative measure of the quality and spread of solutions in the objective space and is calculated as [Cao et al. 2015; Hayes et al. 2022]:

$$\Xi(\mathcal{P}) = \lambda(\theta \in \Theta \mid \exists s \in \mathcal{P}, s \succ x \succ r) \quad (2)$$

where λ denotes the Lebesgue measure.

While hypervolume is widely used in the multi-objective optimisation literature as a combined measure of convergence and spread, it is also influenced by the reference point and the shape of

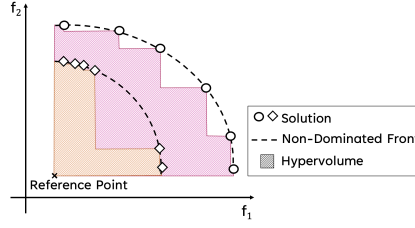


Fig. 2. Two sets of solutions that form different non-dominated fronts as approximations of the true Pareto front. The outer set (marked by circles) achieves a larger hypervolume as it extends further in objective space. Likewise, its sparsity metric is higher, reflecting a more even spread of solutions. Only the outer set of solutions are considered to be non-dominated when the two sets are combined.

the front. For simple linear fronts, hypervolume is maximized by evenly spaced solutions. But on inverted or irregular fronts it may rank boundary solutions more highly, and its evaluation can vary significantly with the choice of reference point, sometimes leading to counter-intuitive comparisons [Ishibuchi et al. 2018; Shang et al. 2021]. We therefore acknowledge these limitations, but we follow prior work in Multi-Objective Quality-Diversity in adopting hypervolume as a standard comparative metric [Janmohamed et al. 2023; Pierrot et al. 2022b].

Sparsity, by contrast, provides complementary information regarding the distribution and evenness of these solutions. It is calculated by evaluating the average nearest neighbour distance among solutions on the front, given by [Hayes et al. 2022]:

$$S(\mathcal{P}) = \frac{1}{|\mathcal{P}| - 1} \sum_{j=1}^m \sum_{i=1}^{|\mathcal{P}|-1} (\tilde{P}_j(i) - \tilde{P}_j(i+1))^2 \quad (3)$$

where $\tilde{P}_j(i)$ denotes the i -th solution of the list of solutions on the front \mathcal{P} , sorted according to the j -th objective and $|\mathcal{P}|$ denotes the number of solutions on the front. To ensure that the sparsity is not skewed due to different scales of each of the objectives, the objective functions must be normalised prior to calculating it. A low-sparsity metric indicates that solutions are well-dispersed through the objective space, highlighting the algorithm's ability to provide diverse trade-off solutions. In contrast, a high-sparsity metric suggests that solutions are clustered in specific regions, potentially indicating that the algorithm struggles to explore and represent the full range of possible trade-offs.

2.3 Multi-Objective Quality-Diversity Algorithms

Multi-Objective Quality-Diversity (MOQD) combines the goals of QD and MO optimisation. Specifically, the goal of MOQD is to return the non-dominated front of solutions in each cell of the feature space with maximum hypervolume, $\mathcal{P}(C_i)$ [Pierrot et al. 2022b]. This MOQD goal can be mathematically formulated as:

$$\max_{\theta \in \Theta} \sum_{i=1}^k \Xi(\mathcal{P}_i), \text{ where } \forall i, \mathcal{P}_i = \mathcal{P}(\theta | \Phi(\theta) \in C_i) \quad (4)$$

MOME [Pierrot et al. 2022b] was the first MOQD algorithm that aimed to achieve this MOQD goal. To achieve this, MOME maintains a non-dominated front in each cell of a MAP-Elites grid. At each iteration, a cell is uniformly selected and then a solution from the corresponding non-dominated front is uniformly selected. Then, the algorithm follows a standard MAP-ELITES procedure: the solution undergoes genetic variation and is evaluated. The evaluated solution is added back to the grid if it lies on the non-dominated front of the cell corresponding to its feature vector.

We note that MOQP differs from related areas such as multi-modal multi-objective optimisation [Li et al. 2023; Liang et al. 2016]. The purpose of multi-modal multi-objective optimisation is to provide a set of equivalent Pareto-optimal outcomes, where each outcome achieves nearly the same balance of objectives but corresponds to a different solution representation, giving end-users flexibility in practice. For example, finding two different circuit layouts that yield the same power–efficiency trade-off, yet offer engineers different implementation choices. In other words, in multi-modal multi-objective optimisation, the goal is to identify multiple Pareto-optimal solutions that are *equivalent in objective space* but differ in decision space. By contrast, MOQP explicitly introduces a feature space $\Phi(\theta)$ that structures the search according to user-defined features. The aim is then to return a Pareto front approximation *within each feature cell*, rather than globally across all solutions. This distinction means that while multi-modal multi-objective optimisation emphasises diversity of solutions that achieve similar trade-offs, MOQP emphasises diversity across features and simultaneously seeks high-performing trade-offs within each feature category.

2.4 Problem Formulation

In this work, we consider an agent sequentially interacting with an environment for an episode of length T , modelled as a Multi-Objective Markov Decision Process (MOMDP), defined by $\langle \mathcal{S}, \mathcal{A}, \mathcal{P}, \mathbf{R}, \Omega \rangle$. At each discrete time step t , the agent observes the current state $s_t \in \mathcal{S}$ and takes an action $a_t \in \mathcal{A}$ by following a policy π_θ parameterized by θ . Consequently, the agent transitions to a new state sampled from the dynamics probability distribution $s_{t+1} \sim p(s_{t+1}|s_t, a_t)$. The agent also receives a reward vector $\mathbf{r}_t = [r_1(s_t, a_t), \dots, r_m(s_t, a_t)]$, where each reward function $r_i : \mathcal{S} \times \mathcal{A} \rightarrow \mathbb{R}$ defines an objective. The multi-objective fitness of a policy π is defined as a vector $\mathbf{F}(\pi) = [f_1(\pi), \dots, f_m(\pi)]$. Here, each f_i represents the expected discounted sum of rewards, calculated as $f_i = \mathbb{E}_\pi [\sum_t \gamma^t r_i(s_t, a_t)]$ for a given reward function r_i . The discount rate $\gamma \in [0, 1]$ controls the relative weighting of immediate and long-term rewards.

2.5 Reinforcement Learning

In the single-objective case ($m = 1$), the MOMDP collapses into a simple Markov Decision Process (MDP) with scalar rewards, where the goal is to find a policy π that maximises the expected discounted sum of rewards or return, $F(\pi) = \mathbb{E}_\pi [\sum_t \gamma^t r(s_t, a_t)]$. Numerous Reinforcement Learning (RL) methods have been developed to address the challenge of finding policies that optimize this cumulative reward. One particularly relevant approach is the Twin Delayed Deep Deterministic Policy Gradient algorithm (TD3)[Fujimoto et al. 2018].

The TD3 algorithm belongs to the broader family of actor-critic RL techniques [Grondman et al. 2012], which involve two key components: an actor network and a critic network. The actor network is a policy parameterised by ϕ , denoted π_ϕ that is used to interact with the environment. The transitions (s_t, a_t, r_t, s_{t+1}) coming from the interactions with the environment are stored in a replay buffer \mathcal{B} and used to train the actor and the critic. The critic network is an action-value function parameterised by ψ , denoted Q_ψ that evaluates the quality of the actor’s actions and helps the agent learn to improve its decisions over time. The critic estimates the expected return obtained when starting from state s , taking action a and following policy π thereafter, $Q_\psi(s, a) = \mathbb{E}_\pi [\sum_t \gamma^t r(s_t, a_t) | s_0 = s, a_0 = a]$.

The TD3 algorithm, uses a pair of critic networks Q_{ψ_1}, Q_{ψ_2} , rather than a single critic network in order to reduce overestimation bias and mitigate bootstrapping errors. These networks are trained using samples (s_t, a_t, r_t, s_{t+1}) from the replay buffer and then regression to the same target:

$$y = r(s_t, a_t) + \gamma \min_{i=1,2} Q_{\psi_i}(s_{t+1}, \pi_{\phi'}(s_{t+1})) + \epsilon \quad (5)$$

where $Q_{\psi'_1}$, $Q_{\psi'_2}$ and $\pi_{\phi'}$ are target networks that are used in order to increase the stability of the training and ϵ is sampled Gaussian noise to improve exploration and smoothing of the actor policy. The actor network is updated to choose actions which lead to higher estimated value according to the first critic network Q_{ψ_1} . This is achieved via a policy gradient (PG) update:

$$\nabla_{\phi} J(\pi_{\phi}) = \mathbb{E} \left[\nabla_{\phi} \pi_{\phi}(s) \nabla_a Q_{\psi_1}(s, a) \mid a = \pi_{\phi}(s) \right] \quad (6)$$

These actor PG updates are executed less frequently than the critic network training in order to enhance training stability.

3 Related Works

3.1 Multi-Objective Evolutionary Algorithms

Multi-Objective Evolutionary Algorithms (MOEA) evolve a population of potential solutions iteratively over several generations to identify an optimal set of solutions that balance conflicting objectives. At each iteration, solutions are selected from the population and undergo genetic variation (through crossover and mutation operators) and are then added back to the population. Different MOEAs can vary in terms of their specific selection strategies, crossover and mutation operators, population management techniques, and how they maintain diversity in the population [Zhou et al. 2011].

Non-dominated Sorting Genetic Algorithm II (NSGA-II) [Deb et al. 2000] and Strength Pareto Evolutionary Algorithm 2 (SPEA2) [Zitzler et al. 2001] both use non-uniform selection mechanisms to guide the optimisation process. Both methods select solutions that are higher performing and occupy less dense regions of the objective space with higher probability. This guides the population towards higher-performing fronts, while simultaneously ensuring solutions are well-distributed across the front.

Our method, MOMe-P2C has synergies with many methods from MOEA literature including non-uniform selection and addition mechanisms (see Section 4.1) and we refer the interested reading to a comprehensive survey of MOEA algorithms for more details [Zhou et al. 2011]. However, we emphasise that MOEA algorithms treat all objectives as quantities to maximise, seeking trade-offs among them. However, in MOQD algorithms, the goal is not to *maximise* feature values but to *cover* the feature space with high-performing solutions. In other words, MOQD algorithms seek solutions which are diverse in the *feature*-space, and then to maximise objectives for each feature. Moreover, our method differs from traditional MOEA approaches in two significant aspects. First, it employs a MAP-ELITES grid to explicitly maintain solutions that are diverse in feature space while optimising over objectives. Second, it incorporates techniques from reinforcement learning to form gradient-based mutations which help to overcome the limited search power of traditional GA variations for high-dimensional search spaces [Nilsson and Cully 2021].

3.2 Multi-Objective Reinforcement Learning

In multi-objective reinforcement learning (MORL) the expected sum of rewards is a vector $J(\pi) = \mathbb{E}_{\pi} [\sum_t \mathbf{r}_t]$. Consequently, there is not a straightforward notion of a reward maximising agent. Single-policy MORL approaches focus on discovering a single policy that achieves a desired trade-off of objectives. Often, this is achieved by employing a scalarization function which transforms the performance on various objectives into a single scalar utility value. For example, many approaches aim to find a policy π that maximises the expected weighted sum of rewards,

$$J(\pi, \omega) = \mathbb{E}_{\pi} \left[\sum_t \omega^{\top} \mathbf{r}_t \right] = \omega^{\top} \mathbb{E}_{\pi} \left[\sum_t \mathbf{r}_t \right] = \omega^{\top} J(\pi) \quad (7)$$

Here, ω is referred to as a *preference*, with $\sum_i \omega_i = 1$. The preference quantifies the relative importance of each of the objective functions and, when the preference is fixed, we can collapse the MOMDP into a single-objective setting that can be optimised with well-established RL approaches.

In single-policy approaches, the challenge arises in determining the preference vector beforehand, as it may prove to be a complex task or may vary among different users [Hayes et al. 2022]. Instead, it may be useful to find solutions which are optimal for different preference values so that the user can examine the range of possible solutions that is on offer and then assign their preferences retrospectively [Hayes et al. 2022]. With this perspective in mind, multi-policy MORL methods aim to find a set of policies that excel across a range of different preferences [Mossalam et al. 2016; Xu et al. 2020]. Often, each policy in the set is trained using preference-conditioned policy-gradient derived from a multi-objective, preference-conditioned action-value function [Mossalam et al. 2016; Xu et al. 2020; Yang et al. 2019].

Some methods straddle the line between single-policy and multi-policy MORL by seeking a single preference-conditioned policy that can maximise the weighted sum of expected returns (Equation (7)) for any given preference [Abels et al. 2019; Parisi et al. 2016; Yang et al. 2019; Zhu et al. 2023]. This approach offers advantages such as reduced storage costs and rapid adaptability [Abels et al. 2019]. However, while having preference-conditioned policy approaches might be cheaper and more flexible, these methods have been observed to achieve worse performance on the objective functions for any given preference than having specialised policies [Xu et al. 2020].

Our work combines elements of both preference-conditioned and multi-policy approaches. Our actor-critic networks are preference-conditioned and are separate from the MAP-ELITES grid. Hence this preference-conditioned actor can be seen as a generalist policy. However, within each cell of the MAP-ELITES grid, we store specialised, non-conditioned policies hence taking a multi-policy approach. To the best of our knowledge, there is no prior research in multi-objective reinforcement learning (MORL) that actively seeks to diversify behaviours in this manner.

3.3 Gradients in Quality-Diversity

QD algorithms belong to the wider class of Genetic Algorithms (GA), which broadly adhere to a common structure of selection, variation and addition to a population of solutions. While these methods have been observed to be highly-effective black box methods, one key limitation is their lack of scalability to high-dimensional search spaces. In tasks in which solutions are the parameters of a neural network, the search space can be thousands of dimensions and thus traditional GA variation operators do not provide sufficient exploration power. To address this, many works in single-objective QD leverage the search power of gradient-based methods in high-dimensional search spaces [Faldor et al. 2023; Flageat et al. 2022; Fontaine and Nikolaidis 2021; Nilsson and Cully 2021; Pierrot et al. 2022a; Tjanaka et al. 2022]. The pioneer of these methods, Policy-gradient assisted MAP-ELITES (PGA-ME) [Nilsson and Cully 2021], combines the TD3 algorithm with the MAP-ELITES algorithms to apply QD to high-dimensional robotics control tasks. In particular, during the evaluation of solutions in PGA-ME, environment transitions are stored and used to train actor and critic networks, using the training procedures explained in Section 2.5. Then, PGA-ME follows a normal MAP-ELITES loop except in each iteration, half of the solutions are mutated via GA variations and the other half are mutated via policy-gradient (PG) updates.

Since PGA-ME, several other QD algorithms with gradient-based variation operators have been proposed. Some of these are tailored to consider different task settings which have differentiable objective and feature functions [Fontaine and Nikolaidis 2021] or discrete action spaces [Boige et al. 2023]. Other methods use policy gradient updates to improve both the fitness *and* diversity of solutions [Fontaine and Nikolaidis 2021; Pierrot et al. 2022a; Tjanaka et al. 2022]. A particular method of note is DCG-ME [Faldor et al. 2023, 2024] which uses policy-gradient variations conditioned

on features of solutions. Similar to MOME-P2C, the motivation for this method is to provide more nuanced gradient information. Conditioning the policy-gradient on the feature value of a solution provides a way to update the solution toward higher performance, *given* that it has a certain behaviour. However, this method only considered mono-objective problems. Other than MOME-PGX (see Section 3.4) we are unaware of gradient-based QD methods applied multi-objective problems.

3.4 Multi-Objective Quality-Diversity Algorithms

Recently, policy gradient variations, inspired by single-objective methods, have played a pivotal role in shaping the development of techniques in MOQD. Notably, while MOME (see Section 3.4) is a simple and effective MOQD approach, it relies on GA policy-gradient mutations as an exploration mechanism which makes it inefficient in high-dimensional search spaces. To overcome this challenge, Multi-Objective MAP-Elites with Policy-Gradient Assistance and Crowding-based Exploration (MOME-PGX) [Janmohamed et al. 2023] was recently introduced as an effort to improve the performance and data-efficiency of MOME in tasks that can be framed as a MOMDP. MOME-PGX maintains an actor and critic network for each objective function separately and uses policy gradient mutation operators in order to drive better exploration in the solution search space. MOME-PGX also uses crowding-based selection and addition mechanisms to bias exploration in sparse regions of the non-dominated front and to maintain a uniform distribution of solutions on the front. MOME-PGX was shown to outperform MOME and other baselines across a suite of multi-objective robotics tasks involving high-dimensional neural network policies. However, since each actor-critic network pair learns about each of the objective separately, the PG variations in MOME-PGX may only provide disjoint gradient information about each of the objectives, and fail to capture nuanced trade-offs.

To the best of our knowledge MOME and MOME-PGX are the only existing MOQD algorithms to date. However, we also note of two particularly relevant approaches which have synergies with the MOQD setting. Multi-Criteria Exploration (MCX) [Gaier et al. 2022] which uses a tournament ranking strategy to condense a solution’s score across multiple objectives into a single value, and then uses a standard MAP-Elites strategy. Similarly, Many-objective Optimisation via Voting for Elites (MOVE) [Dean and Cheney 2023] uses a MAP-Elites grid to find solutions which are high-performing on many-objective problems. In this method, each cell of the grid represents a different subset of objectives and a solution replaces the existing solution in the cell if it is better on at least half of the objectives for the cell. While both MCX and MOVE consider the simultaneous maximisation of many objectives, they both aim to find one solution per cell in the MAP-ELITES grid rather than non-dominated fronts for different features. Therefore, we consider their goals to be fundamentally different from the MOQD goal defined in Equation (4).

Additionally, several works have used multi-objective mechanisms to enhance single-objective QD. These works consider quality (fitness) and diversity directly as optimisation objectives, rather than task-based objectives. For instance, novelty search with local competition [Lehman and Stanley 2011] balances novelty and performance through a multi-objective selection scheme, indicator-based methods [Neumann et al. 2019] employ measures such as hypervolume to guide the spread of solutions, and Pareto-based selection approaches [Do et al. 2024; Wang et al. 2023] explicitly use diversity criteria in archive updates. In all cases, diversity acts as a meta-objective that shapes the search, but the final output remains a single repertoire of diverse, high-quality solutions, in contrast to MOQD which seeks Pareto fronts of task-based trade-offs within each feature.

4 MOME-P2C

In this section, we introduce **Multi-Objective Map-Elites with Preference-Conditioned Policy-Gradient and Crowding Mechanisms (MOME-P2C)**, a new MOQD algorithm that learns a single, preference-conditioned actor-critic framework to provide policy-gradient variations in tasks that

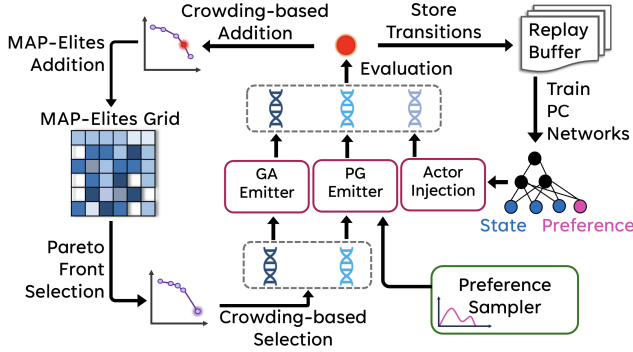


Fig. 3. Overview of MOME-P2C algorithm. Non-dominated Fronts are stored in each cell of a MAP-ELITES grid. At each iteration, a batch of solutions are selected, undergo variation and are added back to the grid based on their performance and crowding-distances. As solutions are evaluated, environment transitions are gathered in a replay buffer and used to train preference-conditioned networks. These networks are used with a preference sampler to perform preference-conditioned PG updates.

can be framed as MDP. The algorithm inherits the core framework of existing MOQD methods, which involves maintaining a non-dominated front within each feature cell of a MAP-ELITES grid and follows a MAP-ELITES loop of selection, variation, and addition for a given budget. Building on the approach of MOME-PGX, our method not only employs traditional genetic variation operators but also integrates policy gradient mutations that improve sample-efficiency, particularly in high-dimensional search spaces. Similar to MOME-PGX, MOME-P2C adopts crowding-based selection, which strategically directs exploration towards less explored areas of the search space and also utilizes crowding-based addition mechanisms to promote a continuous distribution of solutions along the non-dominated front. Distinct from MOME-PGX, which operates with a separate actor-critic framework for each objective function, MOME-P2C innovates by employing a singular, preference-conditioned actor-critic. This design streamlines preference-conditioned policy gradient updates to genotypes, reducing the memory requirements of the algorithm and making it more scalable to problems with a higher number of objectives (a numerical comparison is shown in Section C). Furthermore, MOME-P2C leverages the preference-conditioned actor by injecting it into the main population. A visual representation of the algorithm is depicted in Figure 3, and the accompanying pseudo-code is provided in Algorithm 1. Detailed descriptions of each component of MOME-P2C are available in the following sections.

4.1 Crowding-based Selection and Addition

In MOME-P2C, following MOME-PGX [Janmohamed et al. 2023], we choose to use biased selection and addition mechanisms. In particular, when selecting parent solutions from the grid, we first select a cell with uniform probability and then select an individual from the cell's non-dominated front with probability proportional to its crowding distance. As defined in NSGA-II [Deb et al. 2000], the crowding distance of a solution is defined as the average Manhattan distance between itself and its nearest neighbours on either side of itself in objective space. In MOME-PGX, it was shown that biasing solutions in this manner provides an effective method for guiding the optimisation process toward under-explored regions of the solution space.

Similarly, we also use a crowding-informed addition mechanisms to replace solutions on the non-dominated front. It is important to note that all MOQD methods we consider use a fixed maximum

Algorithm 1 MOME-P2C pseudo-code**Input:**

- MOME archive \mathcal{A} and total number of iterations N
- PG batch size b_p , GA batch size b_g (with $b = b_p + b_g$) and actor injection batch size b_a

// Initialisation

Initialise archive \mathcal{A} with random solutions θ_k

Initialise replay buffer \mathcal{B} with transitions from θ_k

Initialise actor and critic networks $\pi_\phi, Q_{\psi_1}, Q_{\psi_2}$

// Main loop

for $i = 1 \rightarrow N$ **do**

 // Sample solutions

$\theta_1, \dots, \theta_b \leftarrow \text{crowding_selection}(\mathcal{A})$

 // Generate offspring

$\omega_1, \dots, \omega_{b_p} \leftarrow \text{preference_sampler}(\theta_1, \dots, \theta_{b_p})$

$\tilde{\theta}_1, \dots, \tilde{\theta}_{b_p} \leftarrow \text{pg_variation}(\theta_1, \dots, \theta_{b_p}, \omega_1, \dots, \omega_{b_p})$

$\theta_{b_p+1}, \dots, \theta_b \leftarrow \text{ga_variation}(\theta_{b_p+1}, \dots, \theta_b)$

$\omega_{b_p+1}, \dots, \omega_{b_p+b_a} \leftarrow \text{actor_sampler}$

$\theta_{b+1}, \dots, \theta_{b+b_a} \leftarrow \text{actor_inject}(\pi_\phi, \omega_{b_p+1}, \dots, \omega_{b_p+b_a})$

 // Evaluate offspring

$(f_1, \dots, f_m, d, \text{transitions}) \leftarrow \text{evaluate}(\pi_{\tilde{\theta}_1}, \dots, \pi_{\tilde{\theta}_{b+b_a}})$

$\mathcal{B} \leftarrow \text{insert}(\text{transitions})$

$\pi_\phi, Q_{\psi_1}, Q_{\psi_2} \leftarrow \text{train_networks}(\mathcal{B}, \pi_\phi, Q_{\psi_1}, Q_{\psi_2})$

 // Add to archive

$\mathcal{A} \leftarrow \text{crowding_addition}(\theta_{b+1}, \dots, \theta_{b+b_a})$

 // Update iterations

$i \leftarrow i + 1$

return \mathcal{A}

size for the non-dominated front of each cell. This is done in order to exploit the parallelism capabilities of recent hardware advances [Chalumeau et al. 2024; Lim et al. 2022] and consequently affords many thousands of evaluations in a short period of time. However, if a solution is added to a non-dominated front that is at already maximum capacity, another solution must also necessarily be removed. In MOME-P2C, following from MOME-PGX, we remove the solution with the minimum crowding distance in order to increase the sparsity of solutions on the front.

Further details regarding the crowding-based mechanisms can be found in the MOME-PGX paper [Janmohamed et al. 2023]. While we acknowledge that crowding distance may lose effectiveness in many-objective settings [Köppen and Yoshida 2007; Zheng et al. 2024], we adopted it here as a simple and efficient choice consistent with MOME-PGX, and note that it still yields strong results (we include an ablation of the crowding mechanisms in our ablation study Section 6.2.2). Nevertheless,

we note that exploring alternative approaches for preserving diversity of the non-dominated front with a higher number of objectives remains an interesting avenue for future work.

4.2 Preference-Conditioned Actor-Critic

In MOME-PGX, a separate actor-critic framework was used to find a policy π that marginally maximised the expected sum of rewards $J^i(\pi) = \mathbb{E}_\pi[\sum_t r_t^i]$ for each objective $i = 1, \dots, m$. However, in MOME-P2C, we do not require a separate actor-critic framework for each objective function. Instead, we use a *single* actor-critic framework that aims to find a single actor policy to maximise $J(\pi, \omega) = \mathbb{E}_\pi[\sum_t \omega^\top r_t]$ for any given preference ω .

Accordingly, we modify the actor network $\pi_\phi(s)$ to be a conditioned on a preference $\pi_\phi(s|\omega)$. By doing so, the actor network now aims to predict the best action to take from state s_t given that its preference over objectives is ω . In practice, this means that the actor takes its current state s_t concatenated with a preference-vector ω as input, and outputs an action a_t .

Training a preference-conditioned actor requires a corresponding preference-conditioned critic that evaluates the performance of the actor based on the actor's preference. In this setting, we take corresponding preference-conditioned action-value function $Q^\pi(s, a|\omega)$ to be:

$$\begin{aligned} Q^\pi(s, a|\omega) &= \mathbb{E}_{\pi(\cdot|\omega)} \left[\sum_{t=0}^T \gamma^t \omega^\top r(s_t, a_t) \mid s_0 = s, a_0 = a \right] \\ &= \omega^\top \mathbb{E}_{\pi(\cdot|\omega)} \left[\sum_{t=0}^T \gamma^t r(s_t, a_t) \mid s_0 = s, a_0 = a \right] \\ &= \omega^\top Q^\pi(s, a) \end{aligned} \quad (8)$$

Here, $Q^\pi(s, a|\omega)$ denotes the preference-conditioned vectorised action-value function. Equation (8) demonstrates that we can estimate the preference-conditioned action-value function by training a critic $Q_\psi(s, a|\omega) \rightarrow \mathbb{R}^m$ to predict the vectorised action-value function and then weighting its output by the preference. To train this critic network, we modify the target TD3 algorithm given in Equation (5) to be:

$$y = \omega^\top r(s_t, a_t) + \gamma \min_{i=1,2} \omega^\top Q_{\psi_i}(s_{t+1}, \pi_{\phi'}(s_{t+1}|\omega) + \epsilon) \quad (9)$$

which we estimate from minibatches of environment transitions (s_t, a_t, r_t, s_{t+1}) stored in the replay buffer \mathcal{B} .

In order to train the preference-conditioned actor, we use a preference-conditioned version of the policy gradient from Equation (6):

$$\begin{aligned} \nabla_\phi J(\phi, \omega) &= \omega^\top \mathbb{E} \left[\nabla_\phi \pi_\phi(s|\omega) \nabla_a Q_\psi(s, a|\omega) \mid a = \pi_\phi(s|\omega) \right] \\ &= \mathbb{E} \left[\nabla_\phi \pi_\phi(s|\omega) \nabla_a \omega^\top Q_\psi(s, a|\omega) \mid a = \pi_\phi(s|\omega) \right] \end{aligned} \quad (10)$$

The updates of the actor and critic networks, given by Equation (9) and Equation (10), depend on the value of the preference ω . In MOME-P2C, for each sampled transition, we uniformly sample a preference and use this to form a single policy gradient update. Since the preference vector assumes that each of the objectives are scaled equally, we normalise the reward values using a running mean and variance throughout the algorithm. Solutions are stored and added to the archive based on unnormalised fitnesses for interpretability and comparison to other methods.

4.3 Preference-Conditioned Policy Gradient Variation

Given the preference-conditioned actor-critic framework described in Section 4.2, we can form preference-conditioned PG variations on solutions in the archive. In MOME-P2C at each iteration, we

select b_p solutions from the archive and perform n preference-conditioned policy gradient steps. For a given solution θ which parametrises a policy, $\pi_{\theta(s)}$ we update the parameters via:

$$\nabla_{\theta} J(\theta, \omega) = \mathbb{E} \left[\nabla_{\theta} \pi_{\theta}(s) \nabla_a Q_{\psi_1}(s, a | \omega) \Big|_{a=\pi_{\theta}(s)} \right] \quad (11)$$

The PG update given by Equation (11) depends on a preference vector ω . However, it is not straightforward to determine the best strategy for choosing the value of this vector. In this work, we use the term ‘‘PG preference sampler’’ to refer to the strategy we use for determining the preference that the PG variation is conditioned on (illustrated in Figure 3). In MOME-P2C, we choose the PG preference sampler to simply be a random uniform sampler as we found this to be a simple, yet effective strategy. We examine other choices for the PG preference sampler in our ablation study (Section 6.2).

4.4 Actor Injection

In PGA-ME, MOME-PGX and other gradient-based QD methods, the actor policy has the same shape as the policies stored in the MAP-ELITES grid and so can be regularly injected into the main offspring batch as a genotype, with no additional cost to the main algorithm. However, in MOME-P2C, the policies in the MAP-ELITES grid only take the current state s_t as input, whereas the preference-conditioned actor takes the state concatenated with a preference $[s_t, \omega]$ as input. Therefore, the actor has a different architecture to the policies so cannot be added to the repertoire. In this work, we take a similar approach to the one taken by DCRL-ME to inject the conditioned actor within the population [Faldor et al. 2024].

Given the weights $W \in \mathbb{R}^{n \times (|S|+m)}$ and bias $B \in \mathbb{R}^n$ of the first layer of the actor network, we note if we fix the value of ω we can express the value of the n neurons in the first layer as:

$$\begin{aligned} W \begin{bmatrix} s_t \\ \omega \end{bmatrix} + B &= \begin{bmatrix} W_s & W_{\omega} \end{bmatrix} \begin{bmatrix} s_t \\ \omega \end{bmatrix} + B \\ &= W_s s_t + (W_{\omega} \omega + B) \end{aligned} \quad (12)$$

In other words, if the input preference ω to the actor is fixed, we can reshape the preference-conditioned actor network to be the same shape as the policies in the MAP-ELITES grid by absorbing the weights corresponding to the preference input into the bias term of the first layer. This method provides a cheap approach to use the preference-conditioned actor network to generate offspring which have the same shape as other policies in the grid. To take advantage of this in MOME-P2C, at each iteration we sample n_a preferences from an ‘‘actor preference sampler’’ (see Figure 3) and use them to reshape the actor network into n_a new policies. In this work, we choose the actor preference sampler to generate $n_a - m$ uniformly sampled preference vectors for exploration, and m one-hot vectors (with a one at the index for each of the objectives) to ensure that fitness in each of the objectives is always pushed.

5 Experimental Setup

In this section, we describe the evaluation tasks, baselines and metrics we use to evaluate our approach. We introduce two new tri-objective MOQD tasks, ANT-3 and HOPPER-3, which allow us to evaluate the capabilities of different MOQD approaches to scale to a larger number of objectives. We also introduce two new MOQD metrics (MOQD-SPARSITY-SCORE and GLOBAL-SPARSITY) which we argue are important ways to assess whether MOQD algorithms are able to achieve smooth sets of trade-offs. These new tasks and metrics form two key contributions of this work.

Table 1. Summary of evaluation tasks.

						
NAME	ANT-2	ANT-3	HALFCHEETAH-2	HOPPER-2	HOPPER-3	WALKER-2
FEATURE	Feet Contact Proportion					
FEATURE DIM	4		2	1		2
NUMBER OF PARAMETERS	10,312		5,766	5,123		5,702
REWARDS	<ul style="list-style-type: none"> • Forward velocity • Energy consumption 	<ul style="list-style-type: none"> • x velocity • y velocity • Energy consumption 	<ul style="list-style-type: none"> • Forward velocity • Energy consumption 	<ul style="list-style-type: none"> • Forward velocity • Energy consumption 	<ul style="list-style-type: none"> • Forward velocity • Jumping height • Energy consumption 	<ul style="list-style-type: none"> • Forward velocity • Energy consumption

5.1 Evaluation Tasks

We evaluate our approach on six continuous control robotics tasks, which are summarised in Table 1. In these tasks, solutions correspond to the parameters of closed-loop neural network controllers which determine the torque commands given to each of the robot’s joints. In all tasks, the neural network controllers consist of two hidden layers of 64 neurons. The exact number of parameters depends on the observation and action dimensionalities of each environment, as summarised in Table 1. We use four robot morphologies from the Brax suite [Freeman et al. 2021]. In all of the tasks, the feature is the proportion of time that each of the robot’s legs spends in contact with the ground. Given a robot with L legs (summarised in Table 1), the L -dimensional feature space is calculated as:

$$\phi_i(x) = \frac{1}{T} \sum_{t=1}^T c_{i,t} \text{ for } i = 1, \dots, L. \quad (13)$$

Here, $c_{i,t}$ is 1 when the leg is in contact with the ground at time step t , otherwise it is 0. Using this characterisation, solutions that have diverse features will exhibit different gaits [Cully et al. 2015; Pierrot et al. 2022b].

In four of the tasks (ANT-2, HALFCHEETAH-2, HOPPER-2, WALKER-2) the aim is to maximise the forward velocity of the robot while minimising its energy consumption [Janmohamed et al. 2023; Pierrot et al. 2022b]. However, we also introduce two tri-objective MOQD environments: ANT-3 and HOPPER-3. In the ANT-3 task, the objectives are the robot’s x -velocity, y -velocity and energy consumption. Hence the goal is to discover controllers that lead to different gaits, and for each of these gaits to find controllers that travel in different directions while minimising the energy cost. In the HOPPER-3 task, the rewards correspond to the robot’s forward velocity, torso height and energy consumption. The corresponding MOQD goal is to therefore find solutions which have different gaits, and for each of these gaits to find controllers that make the hopper jump to different heights or travel forward, while minimising the energy cost. These tasks were inspired by those in the PG-MORL paper [Xu et al. 2020] but extended to be MOQD problems. We believe that they present interesting and realistic objectives, and also provide opportunity to compare MOQD algorithms on tasks with $m > 2$.

5.2 Baselines

We compare MOME-P2C to seven baselines: MOME-PGX, MOME, PGA-ME, NSGA-II and SPEA2. Despite our best efforts, we were unable to implement PG-MORL as a MORL baseline, as the available code had compatibility issues with the QDax framework [Chalumeau et al. 2024] that we use for parallel evaluations of policies via Brax [Freeman et al. 2021], making PG-MORL more than 250 times slower than the other baselines.

MOME-PGX and MOME are both MOQD algorithms so are straightforward to evaluate. However, NSGA-II and SPEA2 are population-based multi-objective Evolutionary Algorithms (see Section 3.1) which do not explicitly seek diversity and PGA-ME is a mono-objective QD algorithm (see Section 3.3). To evaluate PGA-ME we convert the multiple objectives into a single one by adding them. To ensure that PGA-ME had the same archive size as MOQD methods, if we use a grid of k cells with maximum non-dominated front length of $|\mathcal{P}|$ for MOQD methods, we use $k \times |\mathcal{P}|$ cells for PGA-ME. To ensure that our comparisons are not confounded by differences in archive size, we also include an additional PGA-ME baseline configured with the same number of grid cells as the MOQD methods (see Section D). By contrast, using a large population size for NSGA-II and SPEA2 can reduce selection pressure and limit the number of generations, potentially hindering performance. To address this, we run two versions of both baselines: (1) the NSGA-II and SPEA2 baselines, which use population sizes as close to $k \times |\mathcal{P}|$ that were feasible within our GPU compute limits, and (2) the NSGA-II-SMALL and SPEA2-SMALL baselines, which use the same batch size as the QD baselines but run for more generations to match the total number of evaluations.

To report metrics for PGA-ME, NSGA-II, NSGA-II-SMALL, SPEA2 and SPEA2-SMALL we use a passive archive with the same structure as the MOQD methods. At each iteration, we fill the passive archive with solutions found by the algorithm and then calculate metrics on these archives. Importantly, the passive archives do not interact within the primary algorithmic loop, ensuring that there is no effect on the behaviour of the baseline algorithms.

5.3 Metrics

We evaluate our method based on six metrics:

- (1) The **MOQD-SCORE** [Janmohamed et al. 2023; Pierrot et al. 2022b] is the sum of the hypervolumes of the non-dominated fronts stored in the archive \mathcal{A} :

$$\sum_{i=1}^k \Xi(\mathcal{P}_i), \text{ where } \forall i, \mathcal{P}_i = \mathcal{P}(x \in \mathcal{A} | \Phi(x) \in C_i)$$

This metric aims to assess if an algorithm can find high-performing fronts, for a range of features.

- (2) We introduce the **MOQD-SPARSITY-SCORE**, which we define as the average sparsity of each non-dominated front $\Xi(\mathcal{P}_i)$ of the archive:

$$\frac{1}{k} \sum_{i=1}^k S(\mathcal{P}_i), \text{ where } \forall i, \mathcal{P}_i = \mathcal{P}(x \in \mathcal{A} | \Phi(x) \in C_i)$$

We introduce this metric in MOQD settings as an attempt to measure whether, for each feature, the algorithm succeeds in finding a smooth trade-off of objective functions.

- (3) The **GLOBAL-HYPERVOLUME** is the hypervolume of the non-dominated front formed over all of the solutions in the archive (which we term the *global non-dominated front*). The metric assesses the elitist performance of an algorithm. That is, the performance of solutions on the objective functions that are possible when disregarding the solution's feature.

- (4) By the same reasoning as the **MOQD-SPARSITY-SCORE**, we also introduce the **GLOBAL-SPARSITY**, which is the sparsity of the non-dominated front formed over all of the solutions in the archive.
- (5) We calculated the **MAXIMUM SUM OF SCORES** of objective functions to compare our approach with traditional QD algorithms which directly aim to maximise this.
- (6) The **COVERAGE** is the proportion of cells in of an archive that are occupied. It reflects how many different features the algorithm is able to uncover (regardless of the performance of the solutions). Since all of the algorithms achieved a similar performance on this metric, we report the results for baselines and ablations in Section A .

The MOQD metrics (1 and 2) form evaluation methods that most closely align with assessing whether an algorithm achieves the MOQD goal given by Equation (4). The global metrics (3 and 4) assess the algorithms multi-objective performance, and allow for direct comparison with MO baselines. Since the sparsity metrics can be impacted by imbalanced scales, we run all of the baselines and find the minimum and maximum of the objectives seen across all of the baselines. We then normalise all of the fitnesses based on these values, and report the sparsity metrics based of the final archives from the normalised fitness values.

5.4 Hyperparameters

All experiments were run for the same total budget of of 1,024,000 evaluations. In MOME-P2C, MOME-PGX, MOME, NSGA-II and SPEA2 this corresponded to 4000 iterations with a batch size of 256 evaluations per generation. In NSGA-II-SMALL and SPEA2-SMALL, we used a batch size of 1600 which was the limit of our GPU and ran the algorithm for 640 iterations. We used CVT tessellation [Vassiliades et al. 2018] to create archives with 128 cells, each with a maximum of non-dominated Front length of 50. For all experiments, we use a Iso+LineDD operator [Vassiliades and Mouret 2018] as the GA variation operator, with $\sigma_1 = 0.005$ and $\sigma_2 = 0.05$. This operator mutates a solution by adding isotropic Gaussian noise scaled by σ_1 and a directional perturbation along the vector between two individuals, scaled by σ_2 , promoting both exploration and guided variation. The reference points for each environment and the actor-critic training parameters were kept the same across all algorithms and are provided Section B and Section C.

6 Results

In this section, we present the results for all baselines. Each experiment is replicated 20 times with random seeds. We report p -values based on the Wilcoxon–Mann–Whitney U test with Holm–Bonferroni correction to ensure statistical validation of the results [Holm 1979; Wilcoxon 1992].

6.1 Main Results

The experimental results presented in Figure 4 demonstrate that MOME-P2C outperforms or matches all baselines on all tasks and all metrics. MOME-P2C achieves a significantly higher MOQD-SCORE than all baselines on ANT-2, ANT-3, HALFCHEETAH-2 and HOPPER-3 ($p < 0.02$). MOME-P2C matches the MOQD-SCORE of MOME-PGX, the previous state-of-the-art, on the remaining environments HOPPER-2 and WALKER-2. We include archive visualisations for environments with two-dimensional features in Section E to further visualise these results. Crucially, in the tasks where MOME-P2C does not markedly outperform MOME-PGX on MOQD-SCORE, it still attains lower MOQD-SPARSITY-SCORE (Figure 5), indicating that it achieves smoother array of trade-offs for each feature.

MOME-P2C also outperforms or matches all baselines on the GLOBAL-HYPERVOLUME metric. We include visualisations of the global non-dominated Fronts obtained by representative runs of each of the algorithms in Section F. MOME-P2C outperforms NSGA-II, NSGA-II-SMALL, SPEA2 and SPEA2-SMALL

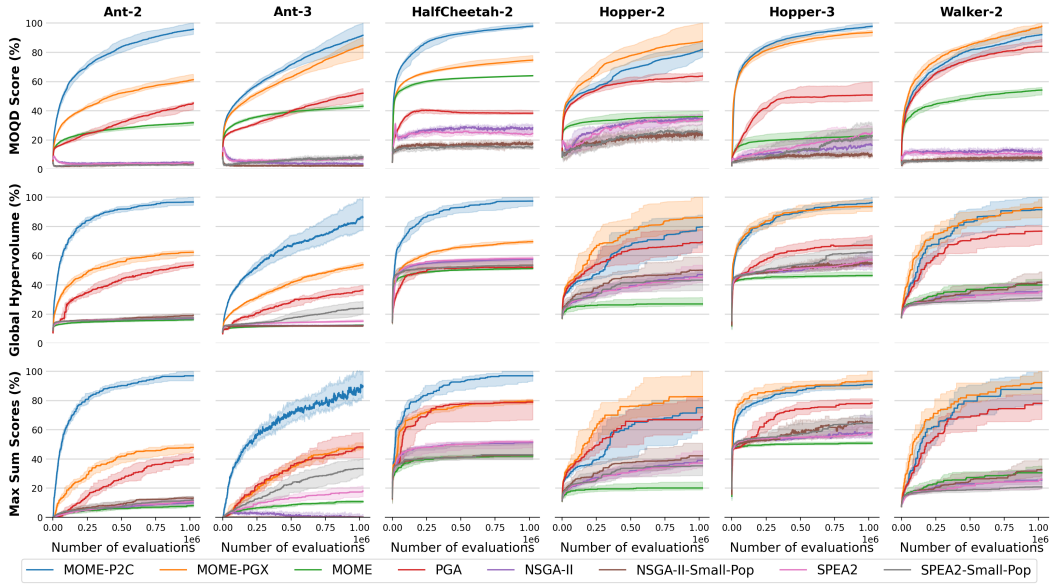


Fig. 4. MOQD-SCORE, GLOBAL-HYPERVOLUME and MAXIMUM SUM OF SCORES (Section 5.3) for MOMe-P2C compared to all baselines across all tasks. Each experiment is replicated 20 times with random seeds. The solid line is the median and the shaded area represents the first and third quartiles.

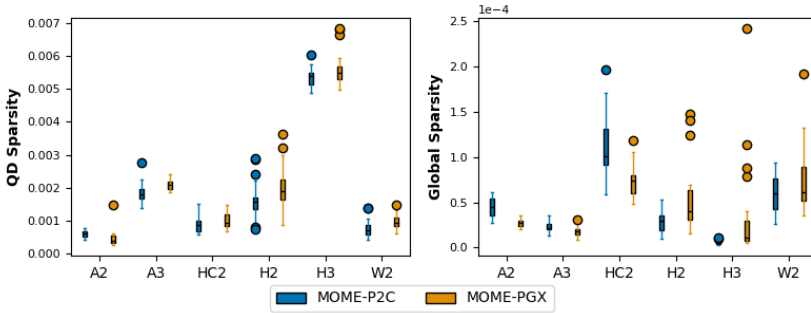


Fig. 5. Boxplots to display sparsity metrics calculated on the final archive of MOMe-P2C and MOMe-PGX over 20 replications. The labels A2, A3, HC2, H2, H3 and W2 correspond to the ANT-2, ANT-3, HALFCHEETAH-2, HOPPER-2, HOPPER-3 and WALKER-2 environments respectively.

on the GLOBAL-HYPERVOLUME in all environments, algorithms that specifically aim to maximise this metric. We hypothesise that this result is due to the policy-gradient variations of MOMe-P2C, which improve the search capabilities of these algorithms in high-dimensional search spaces with neural network controllers. However, MOMe-P2C still outperforms or matches the GLOBAL-HYPERVOLUME of the other baselines which use policy-gradient variations (PGA-ME and MOMe-PGX), demonstrating the benefits of using preference-conditioned updates. Importantly, in the environments where MOMe-P2C matches MOMe-PGX on GLOBAL-HYPERVOLUME (HOPPER-2, HOPPER-3, WALKER-2), it still achieves a lower GLOBAL-SPARSITY as illustrated in Figure 5.

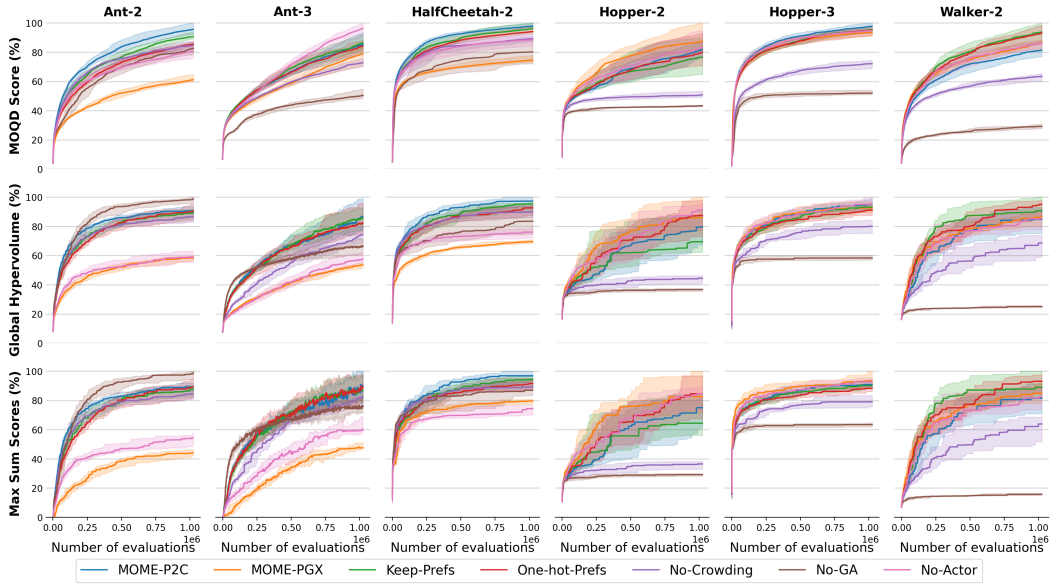


Fig. 6. MOQP-SCORE (Section 5.3) for MOME-P2C compared to all ablations across all tasks. Each experiment is replicated 20 times with random seeds. The solid line is the median and the shaded area represents the first and third quartiles.

Furthermore, MOME-P2C achieves a better MAXIMUM SUM OF SCORES than PGA-ME across all tasks ($p < 10^{-5}$) except HOPPER-2 and WALKER-2 where it still shows improved but not statistically significant performance. This highlights that even if a specific reward preference is available, leveraging multiple objectives may still result in better exploration and higher returns compared to single-objective baselines. Furthermore, we see that MOME-P2C achieves better performance on tri-dimensional tasks, affirming not only its computational efficiency but also its scalability in handling more complex tasks with an increased number of objectives.

6.2 Ablations

6.2.1 Ablation studies. In our ablation studies, we evaluate MOME-P2C against MOME-PGX together with five distinct modifications to understand the contribution of each component in MOME-P2C. These ablations include:

- **KEEP-PREF:** MOME-P2C with a policy-gradient variation operator that keeps the preference of the parent instead of sampling a new preference.
- **ONE-HOT:** MOME-P2C with a policy-gradient variation operator that uses equal batch sizes of one-hot preferences. The ONE-HOT ablation is the same as MOME-PGX except with a preference-conditioned actor-critic network, rather than separate networks.
- **NO-ACTOR:** MOME-P2C without the actor injection mechanism. Instead of generating 64 policy-gradient offspring and 64 actor-injection offspring at each generation, NO-ACTOR produces 128 policy-gradient offspring.
- **NO-GA:** MOME-P2C without any genetic mutations. At each generation, there are 128 policy-gradient offspring and 128 actor-injection offspring.
- **NO-CROWDING:** MOME-P2C without crowding mechanisms, that employs uniform selection and replacement.

6.2.2 Results. The results from our ablation studies provide a deeper understanding of the individual components contributing to MOME-P2C’s effectiveness, we include further archive visualisations in Section E. Firstly, we examine the modifications in preference sampling strategies, as explored in the KEEP-PREF and ONE-HOT ablations. MOME-P2C matches or outperforms the KEEP-PREF ablation, which retains the parent’s preference in the policy-gradient variation operator, across all tasks except WALKER-2. Similarly, the ONE-HOT ablation, employing one-hot preferences in equal batch sizes has no statistical difference or is worse compared to MOME-P2C across all tasks in all metrics except WALKER-2. These results highlight that MOME-P2C is robust to the preference-sampling strategy in most environments. However, the results on WALKER-2 suggests that, in some environments, alternative sampling strategies may be optimal. We leave this as a promising avenue for future research. Additionally, we note that ONE-HOT outperforms or matches MOME-PGX across all metrics, in all environments, highlighting that simply using the preference-conditioned critic leads to improved performance.

The NO-CROWDING ablation, where MOME-P2C operates without its crowding mechanisms, significantly underperforms compared to MOME-P2C across all tasks ($p < 10^{-4}$). This highlights that the crowding-based selection and addition mechanism is crucial for guiding the algorithm towards more diverse and high-quality solutions. Likewise, MOME-P2C also outperforms the NO-GA ablation in every environment except for ANT-2, where the NO-GA ablation environment achieves a higher GLOBAL-HYPERVOLUME and MAXIMUM SUM OF SCORES. We hypothesise that since the Ant robot has higher dimensionality than other morphologies, in this environment the high-dimensionality of the search space requires more gradient-based search power. However, the NO-GA has a worse performance across all other metrics in all of the other environments, particularly HOPPER-2, HOPPER-3 and WALKER-2, highlighting that in general the genetic variations are an essential component of the MOME-P2C algorithm.

Finally, we consider the NO-ACTOR ablation, which removes the actor injection mechanism from MOME-P2C. In the ANT-2 and HALFCHEETAH-2 ($p < 10^{-4}$), MOME-P2C markedly outperforms the NO-ACTOR ablation, suggesting that the actor injection mechanism is essential in these tasks. Moreover, NO-ACTOR either matches or falls behind the full MOME-P2C model in all other tasks and all other metrics, except for the MOQD-SCORE in ANT-3.

7 Conclusion

In this paper, we have introduced a novel algorithm, **MOME-P2C**, which represents a significant advancement in the field of Multi-Objective Quality-Diversity (MOQD) optimisation. Our experiments and ablation studies have demonstrated MOME-P2C’s ability to balance multiple objectives effectively, outperforming existing state-of-the-art methods in challenging continuous control environments.

One of the key strengths of MOME-P2C is its use of preference-conditioned policy gradient mutations, which not only enhance the exploration process but also ensures an even distribution of solutions across the non-dominated front. This approach addresses the limitations of MOME-PGX that struggled with scalability and efficiency. Furthermore, MOME-P2C’s ability to perform well in tri-dimensional tasks highlights its scalability and adaptability to more complex and realistic scenarios.

Beyond these results, a limitation of our study is that experiments were restricted to standard Brax locomotion benchmarks with up to three objectives; extending evaluation to higher-dimensional and non-robotics tasks remains an important avenue for future work. Additionally, a key limitation of MOME-P2C lies in how preferences are currently sampled. While the algorithm is generally robust across environments, certain tasks, such as WALKER-2, demonstrate that naive or uniform preference sampling may be suboptimal. This suggests that dynamic or adaptive sampling strategies could

further improve performance, especially in environments with complex or shifting trade-offs. The exploration of using models to predict which preference will lead to the largest hypervolume gain [Xu et al. 2020] presents an exciting direction for further research.

Finally, while our parameter comparisons in Appendix C demonstrate that MOME-P2C is more memory-efficient than MOME-PGX, scaling to higher-dimensional objective spaces introduces additional challenges. In particular, we expect random preference sampling to become increasingly ineffective as dimensionality grows and, as noted in Section 4.1, crowding distance is known to lose effectiveness in many-objective optimisation [Köppen and Yoshida 2007; Zheng et al. 2024]. Addressing these issues through adaptive preference sampling, scalable diversity-preservation mechanisms, and architectural innovations represents a key line of future work in extending the generality of MOME-P2C.

Acknowledgements

This work was supported by PhD scholarship funding for Hannah from InstaDeep.

References

- Axel Abels, Diederik Roijers, Tom Lenaerts, Ann Nowé, and Denis Steckelmacher. 2019. Dynamic weights in multi-objective deep reinforcement learning. In *International conference on machine learning*. PMLR, 11–20.
- Maxime Allard, Simón C Smith, Konstantinos Chatzilygeroudis, Bryan Lim, and Antoine Cully. 2023. Online damage recovery for physical robots with hierarchical quality-diversity. *ACM Transactions on Evolutionary Learning* 3, 2 (2023), 1–23.
- Varun Bhatt, Bryon Tjanaka, Matthew Fontaine, and Stefanos Nikolaidis. 2022. Deep surrogate assisted generation of environments. *Advances in Neural Information Processing Systems* 35 (2022), 37762–37777.
- Raphaël Boige, Guillaume Richard, Jérémie Dona, Thomas Pierrot, and Antoine Cully. 2023. Gradient-Informed Quality Diversity for the Illumination of Discrete Spaces. In *Proceedings of the Genetic and Evolutionary Computation Conference*. ACM. doi:10.1145/3583131.3590407
- Yongtao Cao, Byran J Smucker, and Timothy J Robinson. 2015. On using the hypervolume indicator to compare Pareto fronts: Applications to multi-criteria optimal experimental design. *Journal of Statistical Planning and Inference* 160 (2015), 60–74.
- Felix Chalumeau, Bryan Lim, Raphael Boige, Maxime Allard, Luca Grillotti, Manon Flageat, Valentin Macé, Guillaume Richard, Arthur Flajole, Thomas Pierrot, et al. 2024. Qdax: A library for quality-diversity and population-based algorithms with hardware acceleration. *Journal of Machine Learning Research* 25, 108 (2024), 1–16.
- Xuxin Cheng, Kexin Shi, Ananye Agarwal, and Deepak Pathak. 2024. Extreme parkour with legged robots. In *2024 IEEE International Conference on Robotics and Automation (ICRA)*. IEEE, 11443–11450.
- Antoine Cully, Jeff Clune, Danesh Tarapore, and Jean-Baptiste Mouret. 2015. Robots that can adapt like animals. *Nature* 521, 7553 (2015), 503–507.
- Antoine Cully and Yiannis Demiris. 2018. Quality and Diversity Optimization: A Unifying Modular Framework. *IEEE Transactions on Evolutionary Computation* 22, 2 (2018), 245–259. doi:10.1109/TEVC.2017.2704781
- Jackson Dean and Nick Cheney. 2023. Many-objective Optimization via Voting for Elites. In *Proceedings of the Companion Conference on Genetic and Evolutionary Computation*. 131–134.
- Kalyanmoy Deb, Samir Agrawal, Amrit Pratap, and Tanaka Meyarivan. 2000. A fast elitist non-dominated sorting genetic algorithm for multi-objective optimization: NSGA-II. In *International conference on parallel problem solving from nature*. Springer, 849–858.
- Anh Viet Do, Mingyu Guo, Aneta Neumann, and Frank Neumann. 2024. Evolutionary Multi-objective Diversity Optimization. In *International Conference on Parallel Problem Solving from Nature*. Springer, 117–134.
- Maxence Faldor, Félix Chalumeau, Manon Flageat, and Antoine Cully. 2023. Map-elites with descriptor-conditioned gradients and archive distillation into a single policy. In *Proceedings of the Genetic and Evolutionary Computation Conference*. 138–146.
- Maxence Faldor, Félix Chalumeau, Manon Flageat, and Antoine Cully. 2024. Synergizing Quality-Diversity with Descriptor-Conditioned Reinforcement Learning. *ACM Trans. Evol. Learn. Optim.* (2024). doi:10.1145/3696426
- Paulo Victor R. Ferreira, Randy Paffenroth, Alexander M. Wyglinski, Timothy M. Hackett, Sven G. Bilen, Richard C. Reinhart, and Dale J. Mortensen. 2019. Reinforcement Learning for Satellite Communications: From LEO to Deep Space Operations. *IEEE Communications Magazine* 57, 5 (2019), 70–75. doi:10.1109/MCOM.2019.1800796

- Manon Flageat, Felix Chalumeau, and Antoine Cully. 2022. Empirical analysis of PGA-MAP-Elites for Neuroevolution in Uncertain Domains. *ACM Transactions on Evolutionary Learning* (2022).
- Matthew Fontaine and Stefanos Nikolaidis. 2021. Differentiable quality diversity. *Advances in Neural Information Processing Systems* 34 (2021), 10040–10052.
- Matthew Fontaine and Stefanos Nikolaidis. 2023. Covariance matrix adaptation map-annealing. In *Proceedings of the genetic and evolutionary computation conference*. 456–465.
- C Daniel Freeman, Erik Frey, Anton Raichuk, Sertan Girgin, Igor Mordatch, and Olivier Bachem. 2021. Brax—A Differentiable Physics Engine for Large Scale Rigid Body Simulation. *arXiv preprint arXiv:2106.13281* (2021).
- Scott Fujimoto, Herke Hoof, and David Meger. 2018. Addressing function approximation error in actor-critic methods. In *International conference on machine learning*. PMLR, 1587–1596.
- Adam Gaier, James Stoddart, Lorenzo Villaggi, and Peter J Bentley. 2022. T-DominO: Exploring multiple criteria with quality-diversity and the tournament dominance objective. In *International Conference on Parallel Problem Solving from Nature*. Springer, 263–277.
- Ivo Grondman, Lucian Busoniu, Gabriel AD Lopes, and Robert Babuska. 2012. A survey of actor-critic reinforcement learning: Standard and natural policy gradients. *IEEE Transactions on Systems, Man, and Cybernetics, Part C (Applications and Reviews)* 42, 6 (2012), 1291–1307.
- Conor F Hayes, Roxana Rădulescu, Eugenio Bargiacchi, Johan Källström, Matthew Macfarlane, Mathieu Reymond, Timothy Verstraeten, Luisa M Zintgraf, Richard Dazeley, Fredrik Heintz, et al. 2022. A practical guide to multi-objective reinforcement learning and planning. *Autonomous Agents and Multi-Agent Systems* 36, 1 (2022), 26.
- Sture Holm. 1979. A simple sequentially rejective multiple test procedure. *Scandinavian journal of statistics* (1979), 65–70.
- Julien Horwood and Emmanuel Noutahi. 2020. Molecular design in synthetically accessible chemical space via deep reinforcement learning. *ACS omega* 5, 51 (2020), 32984–32994.
- Hisao Ishibuchi, Ryo Imada, Yu Setoguchi, and Yusuke Nojima. 2018. How to specify a reference point in hypervolume calculation for fair performance comparison. *Evolutionary computation* 26, 3 (2018), 411–440.
- Hannah Janmohamed, Thomas Pierrot, and Antoine Cully. 2023. Improving the Data Efficiency of Multi-Objective Quality-Diversity through Gradient Assistance and Crowding Exploration. In *Proceedings of the Genetic and Evolutionary Computation Conference*. 165–173.
- Ahmed Khalifa, Scott Lee, Andy Nealen, and Julian Togelius. 2018. Talakat: Bullet hell generation through constrained map-elites. In *Proceedings of The Genetic and Evolutionary Computation Conference*. 1047–1054.
- Elena Krasheninnikova, Javier García, Roberto Maestre, and Fernando Fernández. 2019. Reinforcement learning for pricing strategy optimization in the insurance industry. *Engineering applications of artificial intelligence* 80 (2019), 8–19.
- Mario Köppen and Kaori Yoshida. 2007. Substitute Distance Assignments in NSGA-II for Handling Many-Objective Optimization Problems. In *Evolutionary Multi-Criterion Optimization (EMO) 2007, Lecture Notes in Computer Science*. Vol. 4403. Springer, 727–741.
- Joel Lehman and Kenneth O Stanley. 2011. Evolving a diversity of virtual creatures through novelty search and local competition. In *Proceedings of the 13th annual conference on Genetic and evolutionary computation*. 211–218.
- Wenhua Li, Tao Zhang, Rui Wang, Shengjun Huang, and Jing Liang. 2023. Multimodal multi-objective optimization: Comparative study of the state-of-the-art. *Swarm and Evolutionary Computation* 77 (2023), 101253.
- Jing J Liang, CT Yue, and Bo-Yang Qu. 2016. Multimodal multi-objective optimization: A preliminary study. In *2016 IEEE congress on evolutionary computation (CEC)*. Ieee, 2454–2461.
- Bryan Lim, Maxime Allard, Luca Grillotti, and Antoine Cully. 2022. Accelerated quality-diversity for robotics through massive parallelism. In *ICLR Workshop on Agent Learning in Open-Endedness*.
- Volodymyr Mnih, Koray Kavukcuoglu, David Silver, Alex Graves, Ioannis Antonoglou, Daan Wierstra, and Martin Riedmiller. 2013. Playing Atari with Deep Reinforcement Learning. [arXiv:1312.5602](https://arxiv.org/abs/1312.5602) [cs.LG]
- Hossam Mossalam, Yannis M Assael, Diederik M Roijers, and Shimon Whiteson. 2016. Multi-objective deep reinforcement learning. *arXiv preprint arXiv:1610.02707* (2016).
- Jean-Baptiste Mouret and Jeff Clune. 2015. Illuminating search spaces by mapping elites. *arXiv preprint arXiv:1504.04909* (2015).
- Aneta Neumann, Wanru Gao, Markus Wagner, and Frank Neumann. 2019. Evolutionary diversity optimization using multi-objective indicators. In *Proceedings of the Genetic and Evolutionary Computation Conference*. 837–845.
- Olle Nilsson and Antoine Cully. 2021. Policy gradient assisted map-elites. In *Proceedings of the Genetic and Evolutionary Computation Conference*. 866–875.
- OpenAI, Ilge Akkaya, Marcin Andrychowicz, Maciek Chociej, Mateusz Litwin, Bob McGrew, Arthur Petron, Alex Paino, Matthias Plappert, Glenn Powell, Raphael Ribas, Jonas Schneider, Nikolas Tezak, Jerry Tworek, Peter Welinder, Lilian Weng, Qiming Yuan, Wojciech Zaremba, and Lei Zhang. 2019. Solving Rubik’s Cube with a Robot Hand. [arXiv:1910.07113](https://arxiv.org/abs/1910.07113) [cs.LG]

- Simone Parisi, Matteo Pirota, and Marcello Restelli. 2016. Multi-objective reinforcement learning through continuous pareto manifold approximation. *Journal of Artificial Intelligence Research* 57 (2016), 187–227.
- Thomas Pierrot, Valentin Macé, Felix Chalumeau, Arthur Flajolet, Geoffrey Cideron, Karim Beguir, Antoine Cully, Olivier Sigaud, and Nicolas Perrin-Gilbert. 2022a. Diversity Policy Gradient for Sample Efficient Quality-Diversity Optimization. In *ICLR Workshop on Agent Learning in Open-Endedness*.
- Thomas Pierrot, Guillaume Richard, Karim Beguir, and Antoine Cully. 2022b. Multi-objective quality diversity optimization. In *Proceedings of the Genetic and Evolutionary Computation Conference*. 139–147.
- Justin K Pugh, Lisa B Soros, and Kenneth O Stanley. 2016. Quality diversity: A new frontier for evolutionary computation. *Frontiers in Robotics and AI* 3 (2016), 40.
- Alec Radford, Jong Wook Kim, Chris Hallacy, Aditya Ramesh, Gabriel Goh, Sandhini Agarwal, Girish Sastry, Amanda Askell, Pamela Mishkin, Jack Clark, et al. 2021. Learning transferable visual models from natural language supervision. In *International conference on machine learning*. PmlR, 8748–8763.
- Ke Shang, Hisao Ishibuchi, Linjun He, and Lie Meng Pang. 2021. A Survey on the Hypervolume Indicator in Evolutionary Multiobjective Optimization. *IEEE Transactions on Evolutionary Computation* 25, 1 (2021), 1–20. doi:10.1109/TEVC.2020.3013290
- David Silver, Aja Huang, Chris J Maddison, Arthur Guez, Laurent Sifre, George Van Den Driessche, Julian Schrittwieser, Ioannis Antonoglou, Veda Panneershelvam, Marc Lanctot, et al. 2016. Mastering the game of Go with deep neural networks and tree search. *Nature* 529, 7587 (2016), 484–489.
- Laura Smith, Ilya Kostrikov, and Sergey Levine. 2022. A walk in the park: Learning to walk in 20 minutes with model-free reinforcement learning. *arXiv preprint arXiv:2208.07860* (2022).
- Bryon Tjanaka, Matthew C. Fontaine, Julian Togelius, and Stefanos Nikolaidis. 2022. Approximating Gradients for Differentiable Quality Diversity in Reinforcement Learning. In *Proceedings of the Genetic and Evolutionary Computation Conference (Boston, Massachusetts) (GECCO '22)*. Association for Computing Machinery, New York, NY, USA, 1102–1111. doi:10.1145/3512290.3528705
- Vassilis Vassiliades, Konstantinos Chatzilygeroudis, and Jean-Baptiste Mouret. 2018. Using Centroidal Voronoi Tessellations to Scale Up the Multidimensional Archive of Phenotypic Elites Algorithm. *IEEE Transactions on Evolutionary Computation* 22, 4 (2018), 623–630. doi:10.1109/TEVC.2017.2735550
- Vassiliades Vassiliades and Jean-Baptiste Mouret. 2018. Discovering the elite hypervolume by leveraging interspecies correlation. In *Proceedings of the Genetic and Evolutionary Computation Conference*. 149–156.
- Timothy Verstraeten, Pieter-Jan Daems, Eugenio Bargiacchi, Diederik M Roijers, Pieter JK Libin, and Jan Helsen. 2021. Scalable optimization for wind farm control using coordination graphs. *arXiv preprint arXiv:2101.07844* (2021).
- Ren-Jian Wang, Ke Xue, Haopu Shang, Chao Qian, Haobo Fu, and Qiang Fu. 2023. Multi-objective Optimization-based Selection for Quality-Diversity by Non-surrounded-dominated Sorting. In *IJCAI*. 4335–4343.
- Frank Wilcoxon. 1992. *Individual comparisons by ranking methods*. Springer.
- Jie Xu, Yunsheng Tian, Pingchuan Ma, Daniela Rus, Shinjiro Sueda, and Wojciech Matusik. 2020. Prediction-guided multi-objective reinforcement learning for continuous robot control. In *International conference on machine learning*. PMLR, 10607–10616.
- Runzhe Yang, Xingyuan Sun, and Karthik Narasimhan. 2019. A generalized algorithm for multi-objective reinforcement learning and policy adaptation. *Advances in neural information processing systems* 32 (2019).
- Tom Zahavy, Vivek Veeriah, Shaobo Hou, Kevin Waugh, Matthew Lai, Edouard Leurent, Nenad Tomasev, Lisa Schut, Demis Hassabis, and Satinder Singh. 2023. Diversifying AI: Towards Creative Chess with AlphaZero. arXiv:2308.09175 [cs.AI]
- Qingfu Zhang and Hui Li. 2007. MOEA/D: A multiobjective evolutionary algorithm based on decomposition. *IEEE Transactions on evolutionary computation* 11, 6 (2007), 712–731.
- Weijie Zheng, Yao Gao, and Benjamin Doerr. 2024. A Crowding Distance That Provably Solves the Difficulties of the NSGA-II in Many-Objective Optimization. *arXiv* (2024). <https://arxiv.org/abs/2407.17687> preprint.
- Aimin Zhou, Bo-Yang Qu, Hui Li, Shi-Zheng Zhao, Ponnuthurai Nagarathnam Suganthan, and Qingfu Zhang. 2011. Multiobjective evolutionary algorithms: A survey of the state of the art. *Swarm and Evolutionary Computation* 1, 1 (2011), 32–49. doi:10.1016/j.swevo.2011.03.001
- Baiting Zhu, Meihua Dang, and Aditya Grover. 2023. Scaling Pareto-Efficient Decision Making Via Offline Multi-Objective RL. *arXiv preprint arXiv:2305.00567* (2023).
- Eckart Zitzler, Marco Laumanns, and Lothar Thiele. 2001. SPEA2: Improving the strength Pareto evolutionary algorithm. *TIK-report* 103 (2001).
- Eckart Zitzler and Lothar Thiele. 1998. An evolutionary algorithm for multiobjective optimization: The strength pareto approach. *TIK-report* 43 (1998).

A Coverage Results

Figure 7 and Figure 8 present the coverage results for all of the baseline and ablations algorithms respectively. As expected, all Quality-Diversity algorithms achieve a higher coverage score than the MOEA baselines, as they explicitly seek diverse solutions.

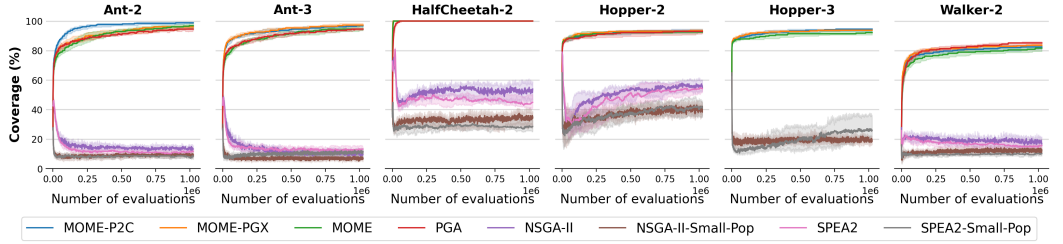


Fig. 7. Median coverage performance of 20 seeds, the shaded regions show the inter-quartile range.

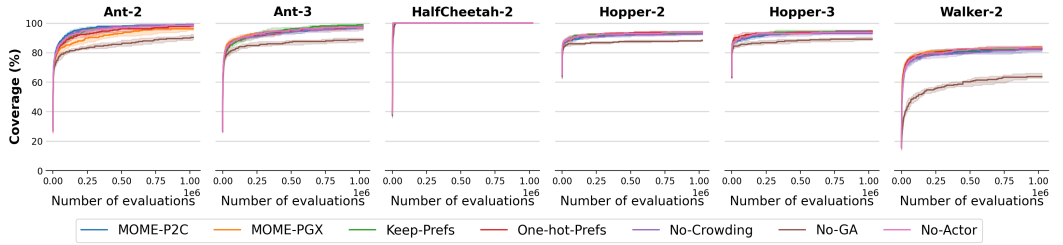


Fig. 8. Median coverage performance of 20 seeds, the shaded regions show the inter-quartile range.

B Hypervolume Reference Points

Table 2 presents the reference points used to calculate the hypervolume metrics in each of the tasks. The same reference points were used for all of the experiments.

Table 2. Reference points

Ant-2	[-350, -4500]
Ant-3	[-1200, -1200, -4500]
HalfCheetah-2	[-2000, -800]
Hopper-2	[-50, -2]
Hopper-3	[-750, -3, 0]
Walker-2	[-210, -15]

C Policy Gradient Hyperparameters

Table 3 presents all of the policy gradient hyperparameters that are used for our algorithms. All hyperparameters were kept the same for each task and for all algorithms which used PG variations.

Table 3. Policy Gradient Network Hyperparameters

Replay buffer size	1,000,000
Critic training batch size	256
Critic layer hidden sizes	[256, 256]
Critic learning rate	3×10^{-4}
Actor learning rate	3×10^{-4}
Policy learning rate	1×10^{-3}
Number of critic training steps	300
Number of policy gradient training steps	100
Policy noise	0.2
Noise clip	0.2
Discount factor	0.99
Soft τ -update proportion	0.005
Policy delay	2

In addition to hyperparameters, we report the number of parameters required for actor and critic networks in MOME-P2C compared to MOME-PGX across all environments. These values directly support the argument in the main text regarding the improved memory efficiency of MOME-P2C.

Table 4. Number of parameters in total for Critic and Actor Networks for MOME-P2C and MOME-PGX in each environment.

	MOME-P2C	MOME-PGX		MOME-P2C	MOME-PGX
ANT-2	182,788	362,500	ANT-2	90,376	180,752
ANT-3	183,814	543,750	ANT-3	90,376	271,128
HALFCHEETAH-2	146,436	289,796	HALFCHEETAH-2	72,198	144,396
HOPPER-2	141,316	279,556	HOPPER-2	69,635	139,270
HOPPER-3	142,342	419,334	HOPPER-3	69,635	208,905
WALKER-2	145,924	288,772	WALKER-2	71,942	143,884

(a) Critic Networks

(b) Actor Networks

As shown, MOME-P2C consistently requires roughly half the number of parameters compared to MOME-PGX across all environments, confirming its memory efficiency advantage. This reduction holds for both actor and critic networks, and becomes more pronounced as the number of objectives increases (e.g., ANT-3 and HOPPER-3). The difference in parameter counts between ANT-2 and ANT-3, and similarly between HOPPER-2 and HOPPER-3, illustrates how scaling to additional objectives affects the two approaches. For MOME-PGX, the number of parameters grows roughly linearly with the number of objectives, since a separate actor-critic pair is maintained for each objective. In contrast, MOME-P2C shows only a marginal increase in parameters between the two- and three-objective tasks, as the same networks are reused and only the input dimensionality grows. This

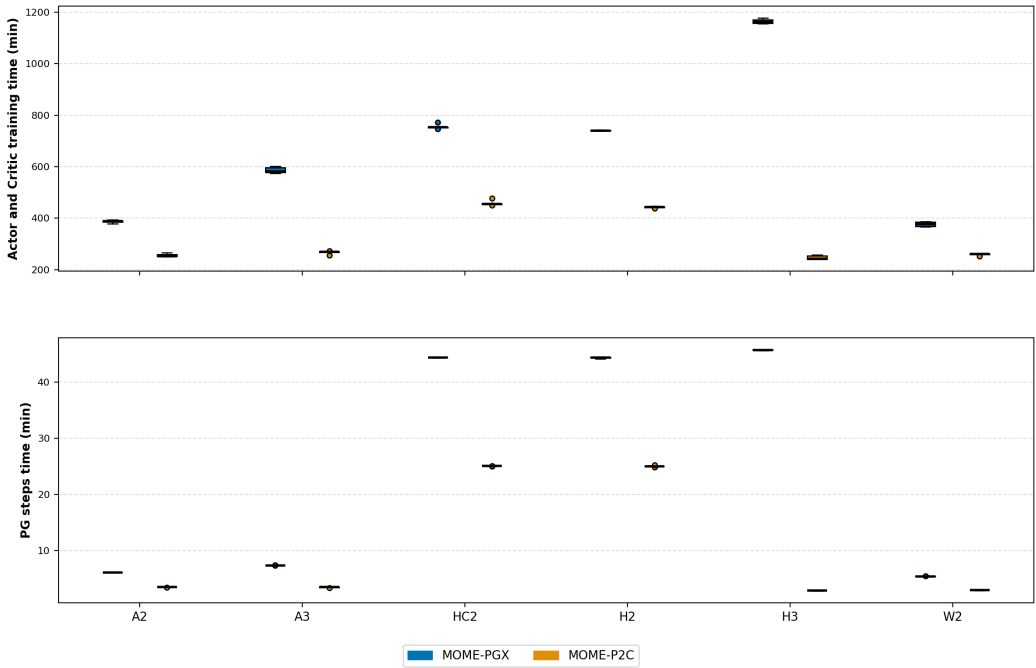


Fig. 9. Wall-clock training time (in minutes) for policy-gradient mutation steps and actor–critic training in each environment. MOME-P2C consistently requires less time than MOME-PGX across all tasks. Note: timings were collected from un-jitted runs for accurate measurement; actual JIT-compiled training is substantially faster.

highlights that while both methods scale with the number of objectives, MOME-P2C’s architecture is more memory-efficient and thus better suited to higher-dimensional problems.

To further support our claims of computational efficiency, Figure 9 reports the wall-clock time of policy-gradient mutation steps and actor–critic training for MOME-P2C and MOME-PGX across all environments. We find that MOME-P2C consistently requires less training time than MOME-PGX in every environment, demonstrating its improved computational efficiency. To obtain accurate timing measurements, we disabled JIT compilation in the QDax framework, as JIT fusion obscures intermediate operation timings. As a result, the reported values are significantly longer than those observed in practice, but they provide a fair relative comparison across methods. In typical JIT-compiled runs, each environment for MOME-P2C completes in under one hour depending on the task. Because un-jitted runs are substantially slower, we report results for five random seeds per environment. Overall, the lower wall-clock times and reduced parameter counts together confirm that MOME-P2C achieves both computational and memory efficiency over MOME-PGX.

D Ablation – Effect of Archive Size for PGA

In the main text, we compared MOME-P2C to PGA-ME using an archive size of $k \times |\mathcal{P}|$ cells, to to ensure a fair comparison in terms of archive capacity. However, having a large number of cells may decrease the selection pressure of the algorithm and therefore negatively impact the performance of PGA-ME. We therefore reran PGA-ME with the same number of grid cells k as the MOQD methods. The results are reported in Figure 10.

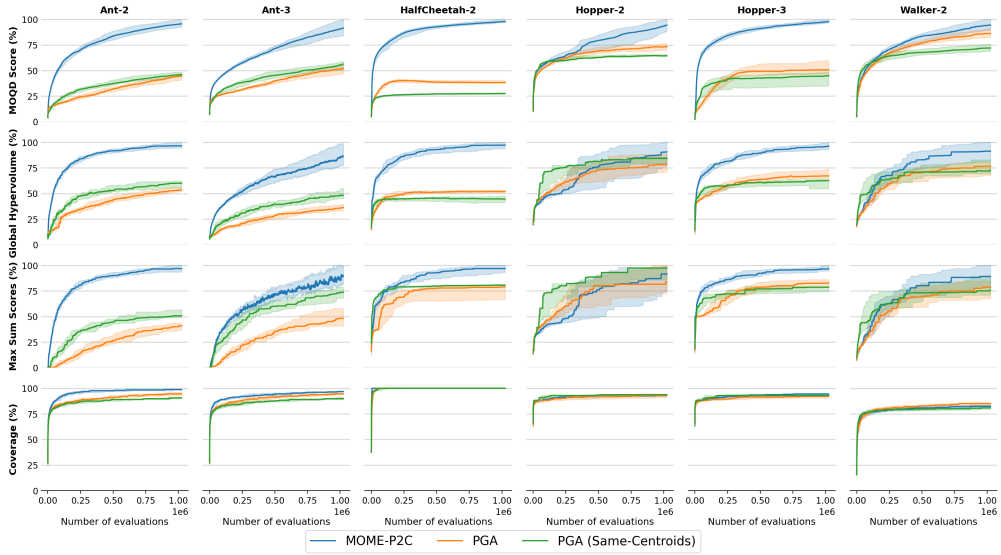


Fig. 10. Comparison between MOE-P2C and PGA-ME when both use the same number of grid cells k . Each curve shows the mean and interquartile range over 20 runs. Results demonstrate that MOE-P2C consistently outperforms or matches PGA-ME across environments, even when controlling for archive size.

We observe that MOE-P2C continues to achieve a higher MOQD-SCORE across all tasks ($p < 0.001$). MOE-P2C also significantly outperforms PGA-ME on the MAXIMUM SUM OF SCORES metrics in most environments, except WALKER-2 and HOPPER-2 where results are not statistically significant. The same trend is observed for the GLOBAL-HYPERVOLUME, where MOE-P2C significantly outperforms PGA-ME on ANT-2, ANT-3, and HALFCHEETAH-2 ($p < 10^{-4}$), as well as HOPPER-3 ($p < 0.01$). Taken together, these results confirm that the observed improvements are not merely an artefact of archive size: even when controlling for the number of cells, MOE-P2C consistently outperforms or matches PGA-ME across environments.

E Repertoire Visualisations

To provide additional insight into the behaviour of the algorithms, we visualise the final repertoires in the feature space for environments with two-dimensional feature descriptors. Figures 11 and 12 show representative seeds for each baseline and ablation, respectively.

In Figure 11, we observe that MOE-P2C produces larger and denser archives with non-dominated fronts with higher hypervolume than the other baselines. Compared to population-based MOEAs such as NSGA-II and SPEA2, which often leave large regions of the feature space unexplored, MOE-P2C and other MOQD algorithms cover the space more uniformly. We also note that the other baselines achieve good coverage, but fail to discover as high-performing fronts as MOE-P2C.

Figure 12 aligns with the quantitative results in Section 6.1, where we observe that in the HALFCHEETAH-2 tasks MOE-P2C performs much better than the ablations, but the ablations are competitive in WALKER-2 environment.

F Global Non-Dominated Fronts

Figure 13 and Figure 14 presents the visualisations of the global non-dominated fronts obtained by each of the baseline and ablation algorithms.

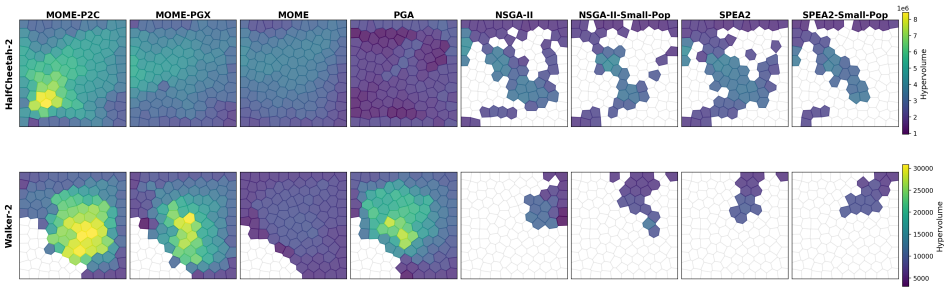


Fig. 11. Representative repertoires for the main baselines in experiments with two-dimensional features. Colours indicate the hypervolume of the non-dominated set in each cell. MOMe-P2c achieves broader coverage and higher-quality solutions compared to other baselines.

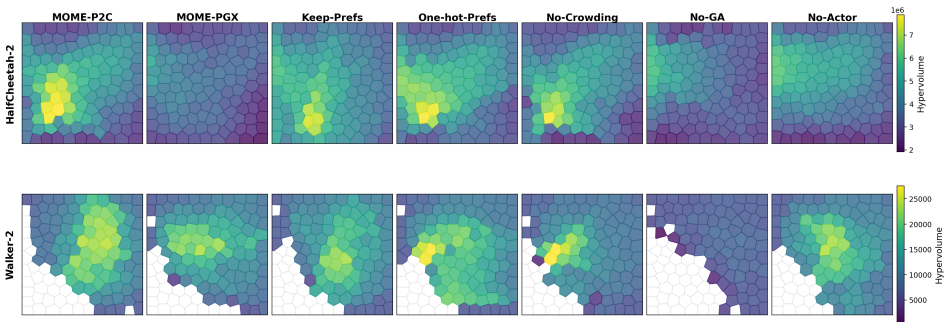


Fig. 12. Representative repertoires for the ablation studies in experiments with two-dimensional features. Each ablation shows a noticeable drop in coverage and/or quality compared to MOMe-P2c, consistent with the quantitative results in the main paper.

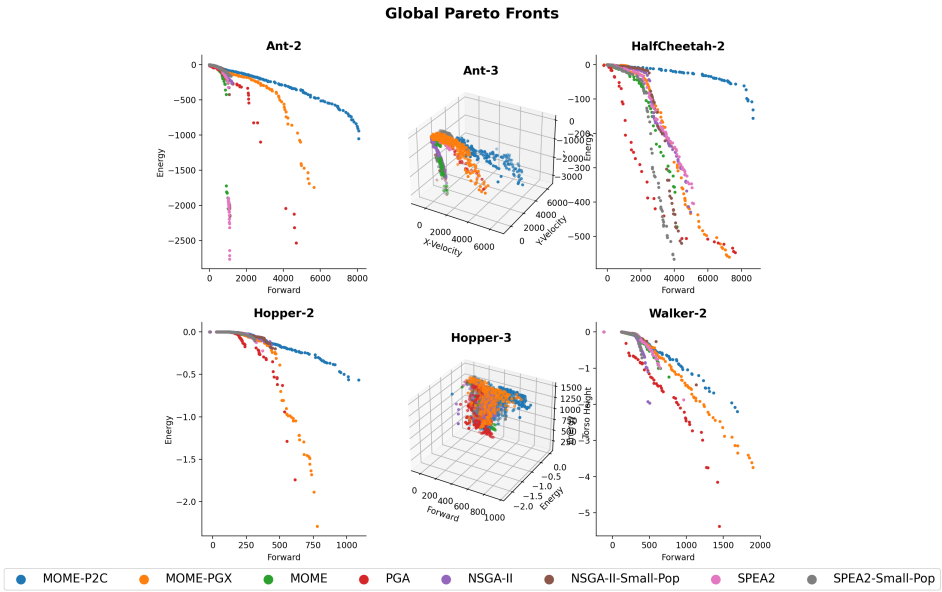


Fig. 13. Visualisations of global non-dominated Fronts obtained by representative runs of each of the baseline algorithms.

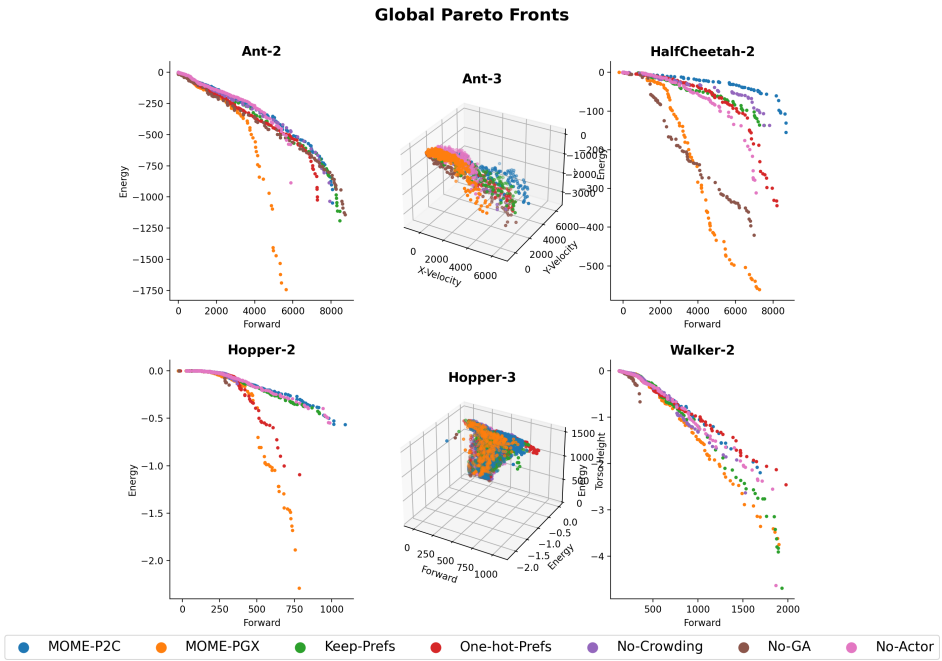


Fig. 14. Visualisations of global non-dominated Fronts obtained by representative runs of each of the ablation algorithms.